JOURNAL OF
Optical Communications
and Networking

Design and evaluation of a reconfigurable optical add-drop multiplexer with flexible wave-band routing in SDM networks

Takuma Kuno,[1,*] Yojiro Mori,[1] Suresh Subramaniam,[2] Masahiko Jinno,[3] and Hiroshi Hasegawa[1]

[1]Department of Information and Communication Engineering, Nagoya University, Furo-cho, Chikusa, Nagoya, 464-8601, Japan
[2]Department of Electrical and Computer Engineering, The George Washington University, 800 22nd Street NW, SEH 6570, Washington DC, 20052, USA
[3]Department of Engineering and Design, Kagawa University, 2217-20 Hayashi-cho, Takamatsu, 761-0396, Japan
*Corresponding author: kuno.takuma.s5@f.mail.nagoya-u.ac.jp

Received 3 December 2021; revised 24 January 2022; accepted 24 January 2022; published 22 February 2022

Space-division multiplexing (SDM) is expected to increase the capacity of photonic networks. Reconfigurable optical add-drop multiplexers (ROADMs) for SDM-based networks must have high scalability in terms of port count. However, the ROADM architecture adopted in present networks cannot support large numbers of ports due to the limited port count of wavelength-selective switches. In this paper, we propose a ROADM architecture composed of space switches and wavelength-routing switches. Space switches have lower per-port cost than wavelength-routing switches. However, space switches cannot route optical paths on a wavelength basis, unlike wavelength-routing switches. By combining these two types of switches, the ROADM port count can be cost-effectively expanded virtually unlimitedly. Numerical simulations show the routing performance of our ROADM; they elucidate that the maximum fiber increment penalty is about 5% compared to the reference scheme. Experiments detail the transmission performance of the ROADM, where 32 Gbaud DP-4QAM/8QAM/16QAM signals are aligned on a 50 GHz grid, are examined.

https://doi.org/10.1364/JOCN.450504

1. INTRODUCTION

Reconfigurable optical add-drop multiplexers (ROADMs) can switch the direction of wavelength-division-multiplexing (WDM) signals without costly optical-electrical and electrical-optical conversion [1–4]. Now that the capacity of single-mode single-core fiber (SCF) is saturating, space-division multiplexing (SDM) technologies using multicore fibers (MCFs) or multiple SCFs are expected to expand network capacity [5–10]. Thus, we need to develop a ROADM architecture that suits SDM networks. The ROADM used in present SCF-based networks is realized by connecting wavelength-selective switches (WSSs) in the route-and-select (R&S) or broadcast-and-select (B&S) manner [11]. In these ROADM architectures, the number of WSSs increases superlinearly with the ROADM port count [12–14]. Therefore, present ROADM architectures are not suitable for SDM networks because they require large numbers of ROADM ports.

Several ROADM architectures for SDM networks have been proposed [15–23]. The fundamental idea behind these architectures is to balance the trade-off between ROADM cost and routing flexibility. One ROADM architecture for SDM networks adopts core-wise switching [15]. In this scheme, inter-core switching within an MCF is abolished to suppress the increase in WSS port count. Although the switchable fibers are limited, the routing performance almost matches that of non-restricted ROADMs. However, many WSSs are still required; for example, $N_f N_c$ $1 \times N_f$ WSSs are needed to form a B&S ROADM, where the number of fibers connected to the ROADM and the number of cores in an MCF are N_f and N_c, respectively. A spatially-jointed switching ROADM, which is another ROADM candidate, can reduce the hardware cost further by abolishing inter-core switching as well as restricting switchable fibers [16–18]. In this scheme, channels that occupy the same frequency slots in an MCF are grouped and treated as a spatial super channel. The hardware cost is low because the spatial super channel is switched by a cost-effective joint-switch (JS) WSS. However, this scheme necessitates high-port-count WSSs because an N_c-array $1 \times N_f$ JS WSS requires $N_c(N_f + 1)$ ports, where the number of cores is N_c and the number of switchable fibers is N_f. Thus, the ROADM is effective on the premise of small N_f and N_c. The other ROADM candidate, fiber-level switching ROADM, reduces the hardware cost by abolishing wavelength-level switching [19]. In this scheme, channels in the same core are grouped

and treated as a spectrum super channel. Spectrum super channels are switched by cost-effective fiber switches based on micro-electro-mechanical systems or piezoelectric actuators. Although flexibility in path routing is severely degraded, the fiber utilization is increased because spectrum fragmentation loss is avoided in high traffic demand scenarios where all available bandwidth in a core is occupied by one optical path. To compose higher-port-count ROADM cost-effectively, we need another solution that eases the trade-off constraint between ROADM cost and routing flexibility.

In hierarchical SDM networks, core-granular routing and wavelength-granular routing are conducted with two types of sub-ROADMs [20–23]. Here, one sub-ROADM is composed of space switches and it can control optical paths on a core basis. The other sub-ROADM is composed of wavelength-routing switches and can control optical paths on a wavelength basis. The use of space switches potentially reduces ROADM cost since space switches have lower per-port cost than WSSs. The inflexibility of space switches is partially offset by the wavelength-routing switches. Thus, combining space switches and wavelength-routing switches is effective in easing the trade-off between ROADM cost and routing performance.

In this paper, we propose a novel ROADM architecture composed of space switches and wavelength-routing switches based on JS WSSs. Following hierarchical SDM networks, the concept of the ROADM is to conduct core-granular routing and wavelength-granular routing with space switches and wavelength-routing switches, respectively. The routing operation is based on flexible wave-band routing (FWBR) [24,25]. With this approach, a high-port-count ROADM can be composed of commercially available low-degree WSSs. Moreover, the port-count of the proposed ROADM can be expanded irrespective of the cost-determining JS WSS scale. Numerical simulations on several network topologies elucidate the feasibility of the proposed scheme. The transmission performance of the ROADM is experimentally evaluated using 96-wavelength dual-polarization (DP) M-ary ($M = 4$, 8, and 16) quadrature amplitude modulation (QAM) signals on the 50 GHz grid. Experiments show that the M-ary QAM signals can traverse 11, 5, and 3 nodes, respectively, where the length of each optical link is set to 100 km. Note that our scheme aims at near-future situations where traffic demands are less than those considered in [19]. In such a case, fiber-level switching suffers a routing penalty because of the lack of the statistical multiplexing effect.

The remainder of this paper is organized as follows: Section 2 explains our proposed ROADM architecture by comparing it with conventional ROADMs. In Section 3, routing characteristics of the ROADM are discussed using the results of network simulations. Section 4 shows measured results of transmission performance. Finally, this paper is concluded in Section 5. Note that preliminary results were presented in conferences [26,27]. This paper provides new numerical simulations and transmission experiments. The transmission experiments in the previous paper did not utilize the full extended C-band due to equipment constraints. In this paper, the transmission experiments examine the full extended C-band of 4.8 THz. We also redid network simulations considering the proposal use in metro networks. As a result, all of the results of this paper are presented for the first time.

2. ROADM ARCHITECTURES

A. ROADM Architecture for SCF-Based Networks

Figure 1 shows two ROADM architectures adopted by existing SCF-based networks [11]. Here, an $N_f \times N_f$ ROADM is assumed, where N_f is the number of single-core fibers. A B&S ROADM consists of $1 \times (N_f + 1)$ optical splitters and $(N_f + 1) \times 1$ WSSs, whereas an R&S ROADM consists of $1 \times (N_f + 1)$ WSSs and $(N_f + 1) \times 1$ WSSs. In both ROADMs, one port of a splitter and a WSS is assigned to an add/drop port. The maximum ROADM port count is bounded because the port count of commercial WSSs is limited to around 35. Although the port count can be expanded by cascading WSSs, the number of costly WSSs increases super-linearly with the ROADM port count [14]. In addition, signals suffer from larger insertion loss of the high-degree optical splitters and severe spectrum narrowing due to the cascaded WSSs.

B. Core-Wise Switching ROADM Architecture

Figure 2 shows the core-wise switching ROADM architecture. Here, an $N_f N_c \times N_f N_c$ ROADM is assumed, where N_f and N_c are the numbers of fibers and cores, respectively. The port count of the ROADM is $N_f N_c$. The ROADM consists of multiple sub-ROADMs. One port of each WSS is used for optical add/drop operation. Each sub-ROADM is dedicated to particular cores labeled with the same number, and hence optical paths can be established between cores that have the same core number. With this approach, the WSS port count can be less than the ROADM port count by limiting switchable cores.

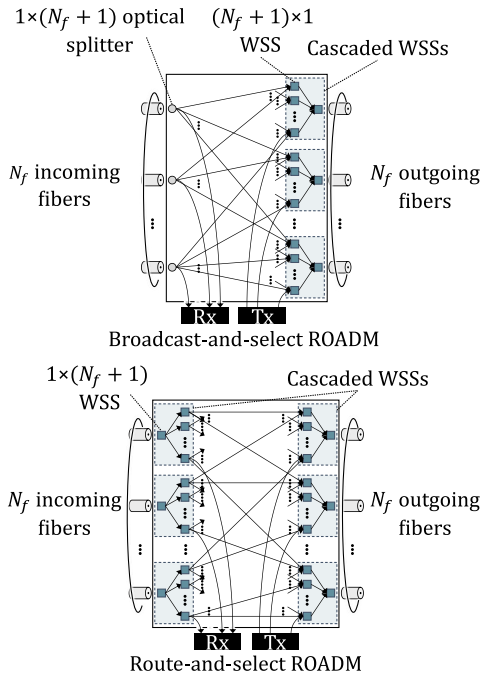

Fig. 1. ROADM architectures for SCF-based networks.

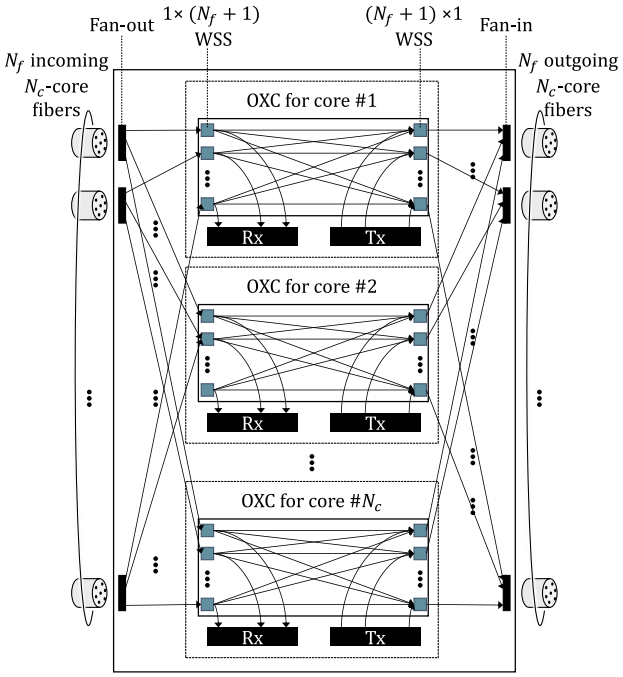

Fig. 2. Core-wise switching ROADM architecture, where R&S ROADMs are exploited as sub-ROADMs.

Despite this limitation, numerical simulations have already proven that the routing performance of the core-wise switching ROADM is almost equal to the performance of non-restricted ROADMs [15].

C. Proposed ROADM Architecture

Figure 3 shows our proposed ROADM architecture consisting of space switches and JS WSSs. Here, n-incoming N_c-core fibers are virtually bundled. $N_b n$ incoming N_c-core fibers and $N_b n$ outgoing N_c-core fibers yield an $N_b N_c n \times N_b N_c n$ ROADM, and the ROADM port count is $N_b N_c n$. The $N_b N_c n \times N_b N_c n$ ROADM consists of $N_b n$ $1 \times N_c$ fan-outs, $N_b N_c n$ 1×2 WSSs, $N_b n$ N_c-array $1 \times B$ JS WSSs, $B N_c n$ $N_b \times N_b$ delivery-and-coupling (DC) space switches, $N_b N_c n$ $(B+1) \times 1$ WSSs, and $N_b n$ $N_c \times 1$ fan-ins. A JS WSS delivers all signals that occupy the same frequency slots in an MCF [16]. In return for the routing constraint, the per-port cost of JS WSSs is low compared to the conventional WSSs deployed in present SCF-based networks. An $N_b \times N_b$ DC space switch consists of N_b $1 \times N_b$ optical selectors and N_b $N_b \times 1$ optical couplers [28]. The switch delivers signals from multiple input ports to each specific output port. The cost of DC space switches is marginal compared to WSSs since they can be cost-effectively fabricated by planar-lightwave-circuit technologies or silicon photonics technologies [28–30]. ROADM routing operation has four steps: First, optical paths are directed to a drop part or an express part by a 1×2 WSS; second, optical paths from MCFs are bundled into B flexible wave bands by an N_c-array $1 \times B$ JS WSS; next, each flexible wave band is guided to a WSS connected to the target core by an $N_b \times N_b$ DC space switch; after that, flexible wave bands and add paths are converged by a $(B+1) \times 1$ WSS. A flexible wave band can be created even if the signal spectra in the wave bands are not adjoining. Demarcations of the flexible wave bands must be set to the same frequency among MCFs connected to the same JS WSS due to the JS WSS constraint. The ROADM port count can be expanded by stacking additional JS WSSs and DC space switches. Thus, the port counts of DC space switches and JS WSSs can be kept constant irrespective of the ROADM port count. Therefore, loss of the ROADM can be kept constant regardless of its port count. Our scheme can also be applied to SCF-based networks since the ROADM part except for fan-outs and fan-ins is comprised of SCFs.

Table 1. Hardware Cost

	Core-wise Switching (B&S)	Proposed scheme
$1 \times (3N_c\text{-}1)$ WSSs Cost : α	$\alpha N_c N_b n \left\lceil \frac{N_b n}{3N_c - 1} \right\rceil$	
1×2 WSSs Cost : β		$\beta N_c N_b n$
N_c-array 1×3 joint-switch WSSs Cost : α		$\alpha N_b n$
1×4 WSSs Cost : γ		$\gamma N_c N_b n$
$N_b \times N_b$ DC space switch Cost : δ		$3\delta N_c n$
Total cost	$\alpha N_c N_b n \left\lceil \frac{N_b n}{3N_c - 1} \right\rceil$	$\alpha N_b n + \beta N_c N_b n + \gamma N_c N_b n + 3\delta N_c n$

Table 1 summarizes the number of necessary WSSs in the core-wise switching ROADM architecture and the proposed ROADM architecture, where their port counts are set to $N_b N_c n \times N_b N_c n$. B is set to 3 because good routing performance can be obtained with three wave bands according to the simulation results in Section 3. For the sake of simplicity, we consider that the cost of a $1 \times (4N_c - 1)$ WSS and that of an N_c-array 1×3 JS WSS are identical. Here, the cost of a $1 \times (4N_c - 1)$ WSS and an N_c array 1×3 joint-switch WSS are expressed as α. The costs of 1×2 WSSs and 1×4 WSSs are expressed as β and γ, respectively. The DC space switch cost is expressed as δ. Note that the DC space switch cost in our proposed ROADM mainly depends on the fabrication cost because the necessary port count of the DC space switch is low, e.g., 4×4. The cost of the ROADM normalized by that of the core-wise switching ROADM is expressed as

$$\frac{\alpha N_f n + \beta N_c N_f n + \gamma N_c N_f n + \delta 3 N_c n}{\alpha N_c N_f n \left\lceil \frac{N_f n}{3N_c - 1} \right\rceil}. \tag{1}$$

Considering that WSS cascading is unnecessary in core-wise switching, $\left\lceil \frac{N_f n}{3N_c - 1} \right\rceil$ is almost 1. Thus, Eq. (1) can be simplified to

$$\frac{1}{N_c} + \frac{\beta + \gamma}{\alpha} + \frac{3\delta}{\alpha N_f}. \tag{2}$$

According to Eq. (2), the proposed ROADM is more effective when the number of cores is large. In addition, the ROADM is effective when the 1×2 WSSs and 1×4 WSSs have lower cost than the $1 \times (4N_c - 1)$ WSS, where the core-wise switching ROADM is composed of multiple B&S ROADMs.

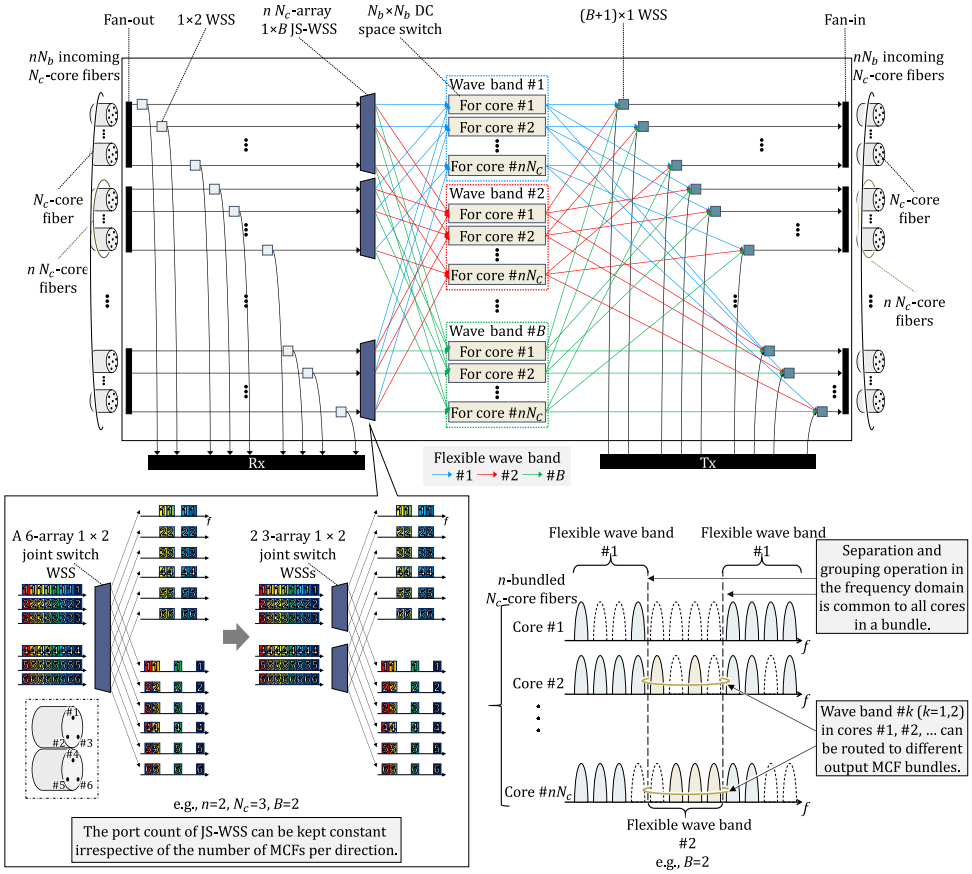

Fig. 3. Proposed ROADM architecture.

3. NETWORK SIMULATIONS

We evaluate the routing performance of the proposed ROADM architecture through computer simulations. Here, we compare the routing performance of ROADMs in terms of the number of fibers required for accommodating a certain amount of traffic. The amount of traffic is given by traffic intensity, which is defined as the average number of optical paths between each node pair. The number of traffic demands is nC_2T, where n and T are the number of nodes and traffic intensity, respectively. Traffic demands are generated as path connection requests whose source and destination nodes are randomly selected following a uniform distribution. Routing is performed by the heuristic algorithm proposed in [24,25]. The algorithm for FWBR is based on the k-shortest path algorithm and minimizes the number of fibers needed to accommodate a given traffic demand in the static network design problem. The baseline for the ROADM is the non-restricted ROADM, which can deliver any wavelength to any core. The route candidates are calculated by the k-shortest path algorithm.

Parameter settings are as follows. The available frequency bandwidth is set to 4.8 THz in the full C-band; i.e., 384 12.5 GHz frequency slots are exploited. We assume three types of optical paths; 4, 7, and 15 slots are allocated to realize 100 Gbps, 400 Gbps, and 1 Tbps, respectively. The path-occurrence probabilities of these demands are 1/3. Considering commercially available devices, the number of cores, N_c, is set to 4 and 7. Twenty trials are performed for each parameter value setting, and the averaged results are shown. Table 2 shows the tested topologies; a 4 × 4 regular-mesh network, Verizon network, and US-metro network are examined [31–33].

Table 2. Tested Physical Topologies

	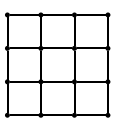	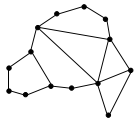	
Network topology	4 × 4 regular-mesh network	Verizon	US metro
Number of nodes	16	14	29
Maximum node degree	4	5	7
Average node degree	3	2.71	2.83

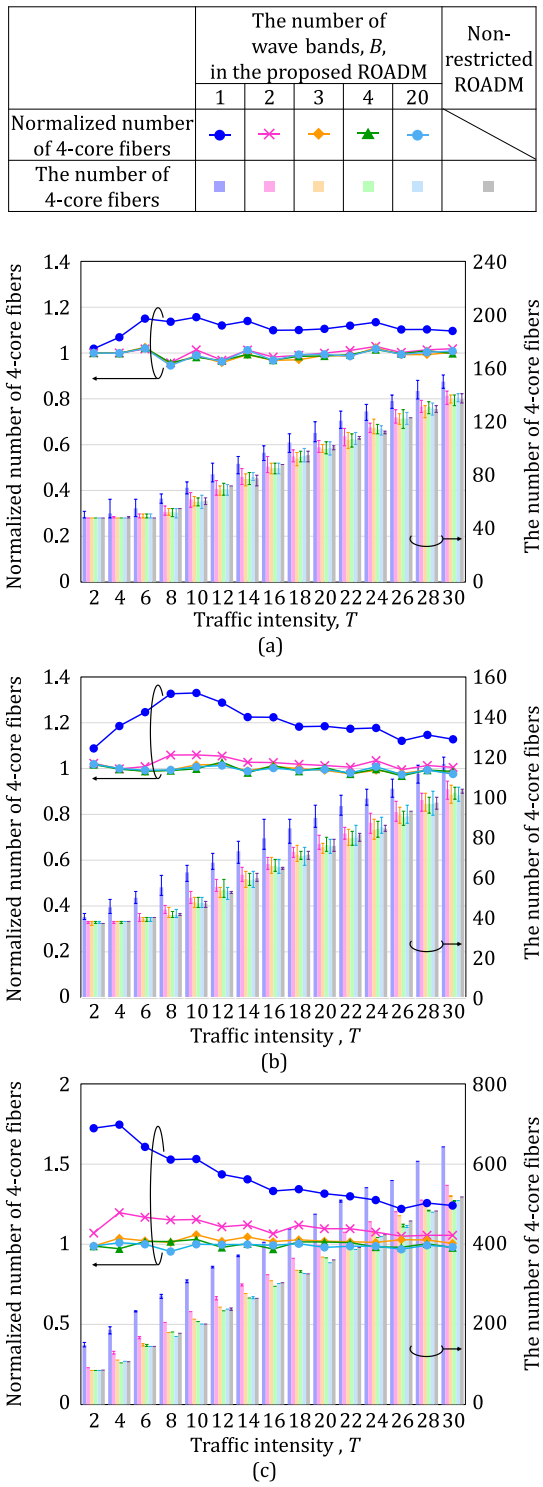

Fig. 4. Number of fibers needed as a function of the traffic intensity, where four-core fibers are assumed. The line graphs indicate the number of four-core fibers, which is normalized by the results of the non-restricted ROADM. The bar graphs indicate the number of four-core fibers. (a) 4×4 regular-mesh network. (b) Verizon network. (c) US metro network.

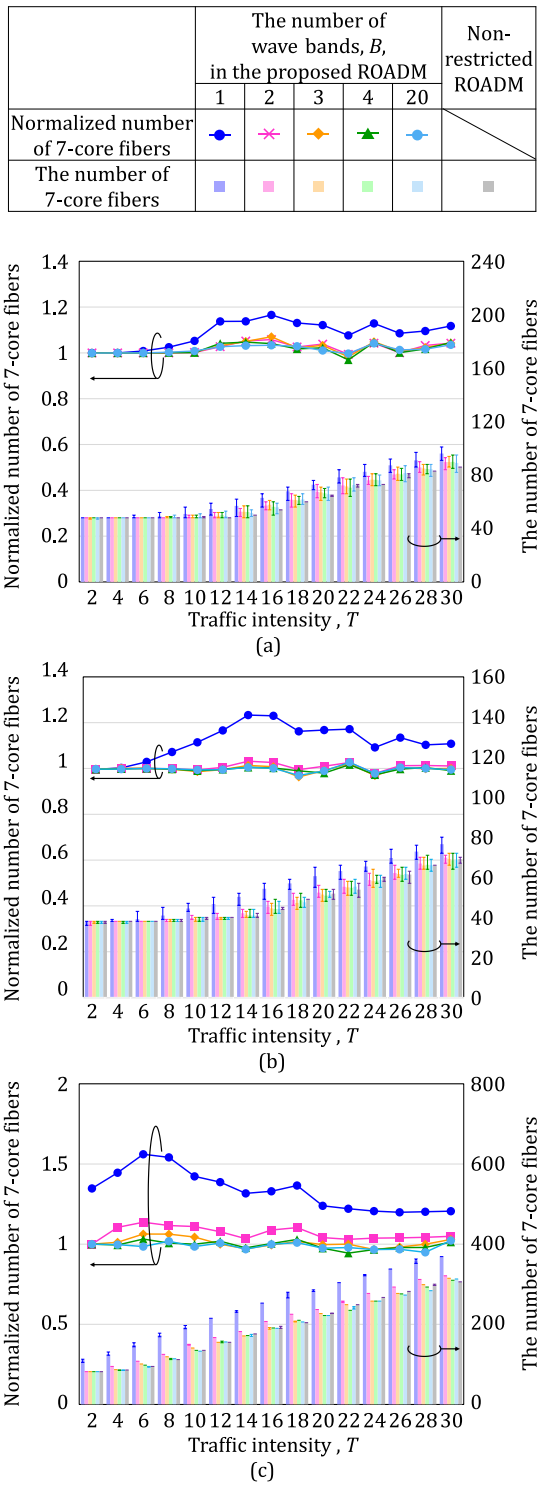

Fig. 5. Number of fibers needed as a function of the traffic intensity, where seven-core fibers are assumed. The line graphs indicate the number of seven-core fibers, which is normalized by the results of the non-restricted ROADM. The bar graphs indicate the number of seven-core fibers. (a) 4×4 regular-mesh network. (b) Verizon network. (c) US metro network.

Figure 4 shows the number of fibers versus traffic intensity T, where the use of four-core fibers is assumed. The bar graphs depict the number of fibers, and their largest and smallest values are indicated by error bars. When the traffic intensity is small, the increment of the numbers of fibers is gradual because there is a sufficient number of fibers to accommodate optical

paths. The line graph shows the number of fibers, which is normalized by the results of the non-restricted ROADM. The curve of FWBR with larger numbers of wave bands approaches the curve of the non-restricted ROADM. When the number of wave bands B is set to 2 or more, the routing penalty is less than 5% in the 4×4 regular-mesh network and Verizon network. This indicates that the proposed ROADM accommodates 95% of traffic in the networks compared to a core-wise switching ROADM in these topologies. Considering the present traffic increase rate of 1.3/year, a 5% traffic increase corresponds to a two-month advance in the fiber laying schedule. Regarding the US-metro network, the maximum fiber increment penalty is around 5% when B is set to 3 or more. If the number of nodes in a network is large, required WSS degree B becomes large. However, reducing B is needed for lowering the node cost. Thus, B should be decided considering the fiber cost and the node cost.

Figure 5 shows simulation results, where the use of seven-core fibers is assumed. The fiber increment penalty is less than 5% in the 4×4 regular-mesh network and Verizon network when B is set to 2 or more. Regarding the US metro network, the fiber increment penalty is around 5% when B is set to 3. The fiber increment penalties tend to be smaller compared to Fig. 4 because the increased number of cores reduces the number of fibers needed. All results indicate that 2 or 3 wave bands is sufficient for attaining good routing performance. Thus, the use of the proposed ROADM architecture enables us to reduce the ROADM cost in return for a fiber increment of a few percent.

Figure 6 shows the fiber utilization ratio versus traffic intensity, where the use of four-core fibers and seven-core fibers are assumed. The fiber utilization ratio is defined as the number of occupied slots divided by the number of slots in the network. In the small traffic intensity area, the deviation of the curve with one flexible wave band and those of others are small because sufficient free slots exist for accommodating optical paths. In the high traffic intensity area, the use of FWBR enhances the fiber utilization efficiency. FWBR makes the wavelength resources available to B switchable fibers, where B is the number of flexible wave bands. The route candidates in the non-restricted ROADM would be small in the larger traffic area, and hence similar routing performance can be obtained with a few wave bands.

4. TRANSMISSION EXPERIMENTS

To evaluate the transmission performance of our ROADM architecture, we conducted proof-of-concept transmission experiments. We used SCFs as transmission links; however, similar results are expected to be obtained with MCFs because seven-core fibers whose cross talk was estimated to be less than -30 dB after 1.4×10^3 km transmission have already been reported [34]. Thus, inter-core cross talk is negligible in metro networks, which is our target. Figure 7 shows the experimental setup. At the transmitter, a continuous wave (CW) was generated by a tunable wavelength laser. The CW was modulated to 32 Gbaud M-ary QAM ($M = 4$, 8, or 16) signal by a lithium-niobate IQ modulator (IQM) driven by an arbitrary-waveform generator (AWG). After amplification by a polarization-maintaining (PM) erbium-doped fiber amplifier (EDFA), the DP M-ary QAM signal was created by a polarization-division multiplexing (PDM) emulator comprised of a polarization-beam splitter (PBS), a 10-ns-delay fiber, and a polarization-beam combiner (PBC). As non-target signals, 95-wavelength 32 Gbaud DP-M-ary QAM signals were generated by using a 95-CW source, an IQM, and a PDM emulator. After that, the signals were amplified by a PM EDFA. With a 3×1 WSS, the target signal and the non-target signals were converged, and we obtained 96 channels of 32 Gbaud DP-M-ary QAM signals aligned on a 50 GHz grid. In addition, the noise added on the same frequency slots with the target signal was eliminated. The signal power was adjusted by an EDFA and variable optical attenuator (VOA). To attain flat WDM signals, the signal power was shaped by a WSS considering the signal spectrum after EDFA traversal. The signals entered a loop consisting of a 2×2 optical splitter, a 100 km SMF, an EDFA, the ROADM under test, an EDFA, a VOA, and two synthesized switches (SWs). Note that loss due to fan-out/in is included in the VOA loss. The loss coefficient, nonlinearity coefficient, and dispersion parameter of the SCF were 0.18 dB/km, 1.5/W/km, and 16.5 ps/nm/km, respectively. The noise figure of the EDFAs was around 5 dB. The ROADM consisted of a 1×2 WSS, a seven-array 1×2 JS WSS, a $1 \times N$ optical selector, a VOA, and a 3×1 WSS. The losses of a 1×2 WSS, a seven-array 1×2 JS WSS, a $1 \times N$ optical selector, and a 1×3 WSS were 6.3 dB, 7.9 dB, 1.4 dB, and 6.4 dB, respectively. The $N \times N$ DC space switch was emulated by combining a $1 \times N$ optical selector and a VOA. The loss of the optical coupler emulated by the VOA was parameterized. We assumed the use of two wave bands. The target and non-target signals were separated by the 1×2 WSS. The target signal was delivered to the $N \times N$ DC space switch, and non-target signals were dropped. Target and non-target signals were converged at the 3×1 WSS. Thus, the target signal is impaired by spectrum narrowing 3 times in each ROADM traversal. Note that cross talk in our proposed ROADM can be small unlike the large cross talk of the typical large-scale ROADMs. This is because our architecture does not adopt full-mesh connectivity. The numbers of non-target ports that generate cross talk are $N_c - 1$ at an N_c-array $1 \times B$ JS WSS, $N_b - 1$ at an $N_b \times N_b$ DC switch, and B at a $(B + 1) \times 1$ WSS. In a typical case, $N_c - 1 = 6$, $N_b - 1 = 3$, and $B = 2$, and hence cross talk is much smaller than that of the full-mesh architecture. In this way, cross talk is significantly reduced thanks to the coarse port connectivity adopted in our ROADM. The signal power was optimized by the EDFA and the VOA. To flatten the WDM signals, the power of the non-target signals was shaped by the 3×1 WSS considering the signal spectrum after EDFA traversal. The output power of the EDFA before ROADM traversal P_{in} was set to 9 dBm per wavelength; note that the EDFA power was set to such a high power to examine a wide measurement region. After multiple loops, the route of signals was switched, and the signals entered a 100 km SMF. Finally, signals were dropped by a 1×2 WSS and coherently detected. The digital signal processing circuit in the digital coherent receiver performed polarization recovery, carrier-phase estimation, frequency estimation, receiver-side

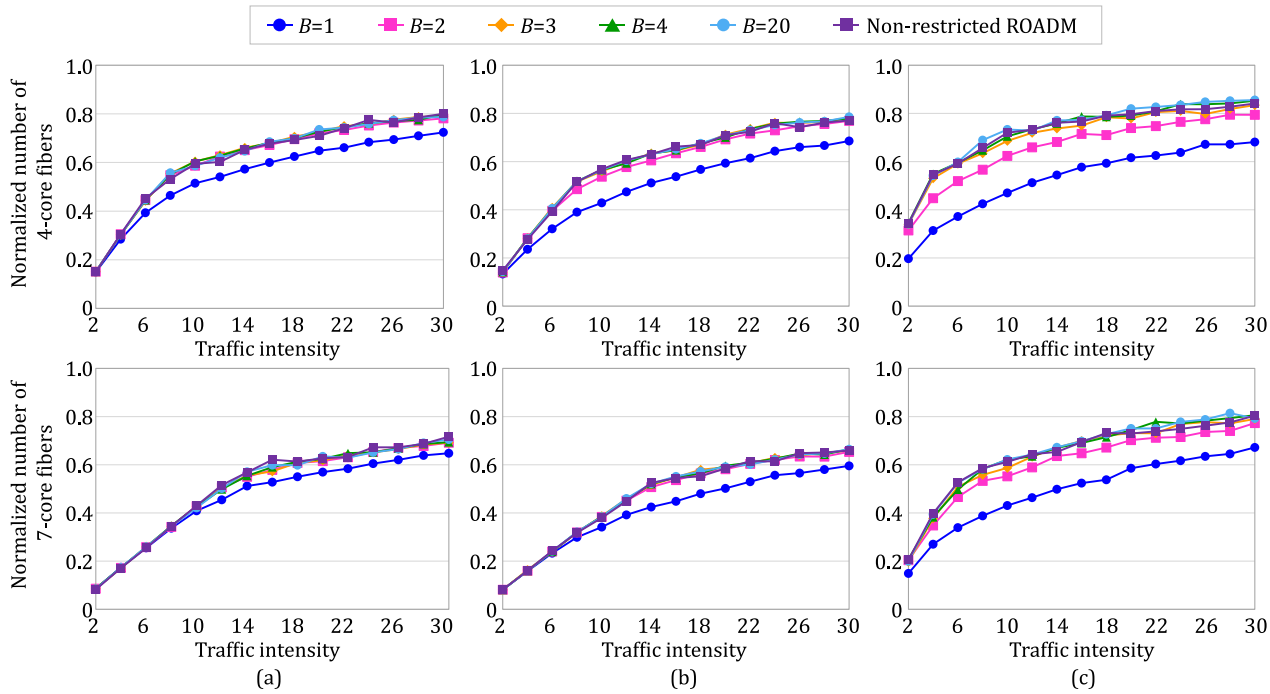

Fig. 6. Fiber utilization ratio versus traffic intensity. (a) 4 × 4 regular-mesh network. (b) Verizon network. (c) US metro network.

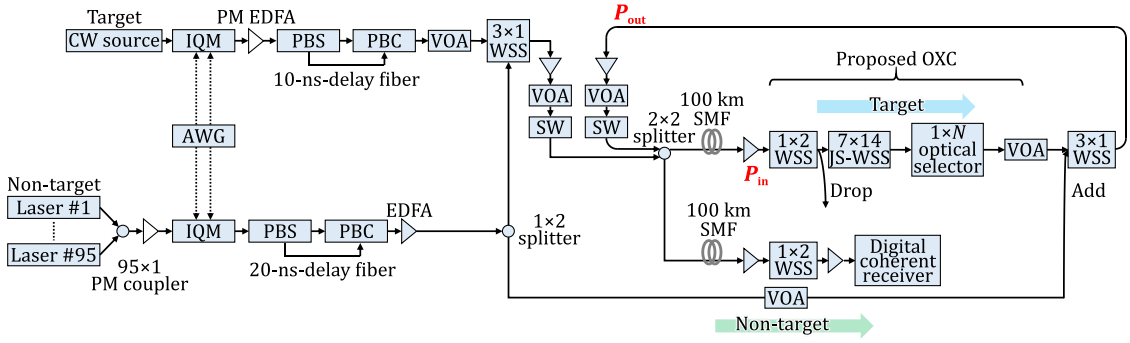

IQM	IQ modulator	WSS	Wavelength selective switch
AWG	Arbitrary waveform generator	SW	Switch
PM EDFA	Polarization-maintaining erbium-doped fiber amplifier	EDFA	Erbium-doped fiber amplifier
PBS	Polarization beam splitter	SMF	Single-mode fiber
PBC	Polarization beam combiner	JS-WSS	Joint-switch wavelength-selective switch
VOA	Variable optical attenuator		

Fig. 7. Experimental setup.

IQ related impairments compensation, and symbol decoding [35,36]. Note that the SNR determiner of the ROADM is the signal power per wavelength after ROADM traversal, P_{out}. Investigating the relationship between P_{out} and the bit-error ratio (BER) yielded a graph of the transmissible distance versus the DC space switch scale.

Figure 8 plots the BER versus hop count, where the loss caused by DC space switches is parameterized. Assuming the use of forward error correction, the acceptable BER threshold was set to 2.7×10^{-2} [37]. When P_{out} is set to −2.7 dBm, 4QAM, 8QAM, and 16QAM signals can hop 11, 5, and 3 nodes, respectively. This yields distances of 1100, 500, and 300 km, respectively. These results indicate that our proposed ROADM can be applied to metro networks with reasonable hardware requirements. Note that this experiment was conducted under the worst case where the signal is impaired by spectrum narrowing at every node hop. Thus, the maximum transmission distance and maximum hop count can be extended if impairment-aware routing and spectrum assignment algorithms are applied [38].

Figure 9 shows the necessary node input power P_{in} to attain the target transmission distance L, when a specific DC switch scale is used. For example, P_{in} of 4QAM signals must be larger than 2 dBm when the target transmission distance is 1100 km and the DC switch scale of 4 × 4 is used. These results are useful in designing networks. Note that

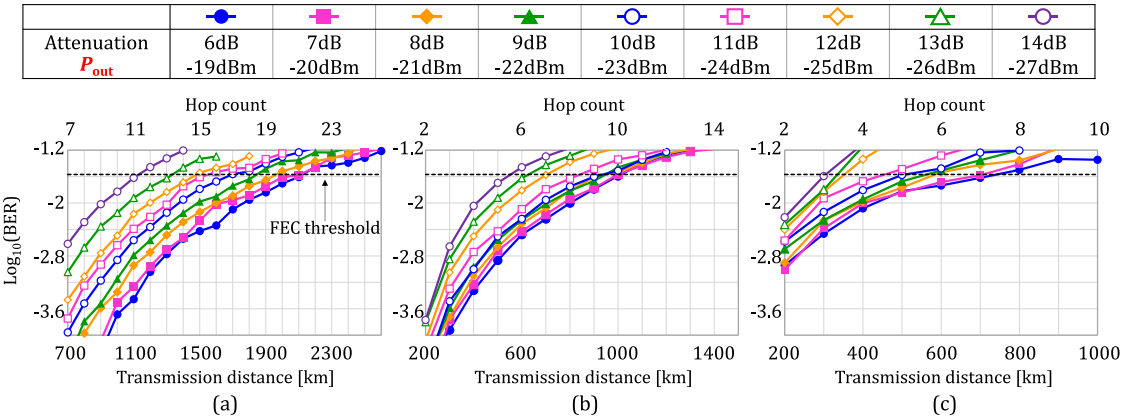

Fig. 8. BER characteristics versus transmission distance.

4QAM		P_{in} [dBm]								
		9	8	7	6	5	4	3	2	1
Transmission distance, L [km]	700	19×19	15×15	12×12	10×10	7×7	6×6	5×5	4×4	3×3
	800	19×19	15×15	12×12	10×10	7×7	6×6	5×5	4×4	3×3
	900	19×19	15×15	12×12	10×10	7×7	6×6	5×5	4×4	3×3
	1000	19×19	15×15	12×12	10×10	7×7	6×6	5×5	4×4	3×3
	1100	19×19	15×15	12×12	10×10	7×7	6×6	5×5	4×4	3×3
	1200	15×15	12×12	10×10	7×7	6×6	5×5	4×4	3×3	
	1300	15×15	12×12	10×10	7×7	6×6	5×5	4×4	3×3	
	1400	12×12	10×10	7×7	6×6	5×5	4×4	3×3		
	1500	10×10	7×7	6×6	5×5	4×4	3×3			
	1600	7×7	6×6	5×5	4×4	3×3				
	1700	6×6	5×5	4×4	3×3					
	1800	6×6	5×5	4×4	3×3					
	1900	5×5	4×4	3×3						
	2000	4×4	3×3							
	2100	4×4	3×3							

8QAM		P_{in} [dBm]								
		9	8	7	6	5	4	3	2	1
Transmission distance, L [km]	200	19×19	15×15	12×12	10×10	7×7	6×6	5×5	4×4	3×3
	300	19×19	15×15	12×12	10×10	7×7	6×6	5×5	4×4	3×3
	400	19×19	15×15	12×12	10×10	7×7	6×6	5×5	4×4	3×3
	500	19×19	15×15	12×12	10×10	7×7	6×6	5×5	4×4	3×3
	600	15×15	12×12	10×10	7×7	6×6	5×5	4×4	3×3	
	700	12×12	10×10	7×7	6×6	5×5	4×4	3×3		
	800	10×10	7×7	6×6	5×5	4×4	3×3			
	900	7×7	6×6	5×5	4×4	3×3				
	1000	3×3								

16QAM		P_{in} [dBm]								
		9	8	7	6	5	4	3	2	1
Transmission distance, L [km]	200	19×19	15×15	12×12	10×10	7×7	6×6	5×5	4×4	3×3
	300	19×19	15×15	12×12	10×10	7×7	6×6	5×5	4×4	3×3
	400	10×10	7×7	6×6	5×5	4×4	3×3			
	500	7×7	6×6	5×5	4×4	3×3				
	600	4×4	3×3							
	700	4×4	3×3							

Fig. 9. Attainable maximum scale of the DC space switch.

the loss of the DC space switch including excess loss is set to $10\log_{10}(N_b) + 2.4$ dB, where N_b is the DC space switch scale; $10\log_{10}(N_b)$ corresponds to the theoretical loss of an optical coupler. Optical selector loss and excess loss are set to 1.4 dB and 1 dB, respectively.

5. CONCLUSION

We proposed a high-port-count ROADM architecture that consists of JS WSSs and DC space switches. By using space switches and JS WSSs to realize flexible wave-band routing, the ROADM port count in terms of the number of cores connected to the ROADM can be cost-effectively increased while keeping acceptable routing performance. Furthermore, the ROADM port count can be expanded without increasing the JS WSS port count. Network simulations elucidated that the routing penalty is about 5% with a few-degree JS WSS in every topology examined. Transmission experiments demonstrated that the proposed ROADM can cover most metro networks. Our cost-effective ROADM architecture will contribute to realizing future SDM networks.

Funding. National Institute of Information and Communications Technology.

REFERENCES

1. A. Watanabe, S. Okamoto, and K. Sato, "Optical path cross-connect node architecture with high modularity for photonic transport networks," IEICE Trans. Commun. **E77-B**, 1220–1229 (1994).
2. J. Strand and A. Chiu, "Realizing the advantages of optical reconfigurability and restoration with integrated optical cross-connects," J. Lightwave Technol. **21**, 2871–2882 (2003).
3. M. Jinno, H. Takara, B. Kozicki, Y. Tsukishima, Y. Sone, and S. Matsuoka, "Spectrum-efficient and scalable elastic optical path network: architecture, benefits, and enabling technologies," IEEE Commun. Mag. **47**(11), 66–73 (2009).
4. R. Hashimoto, S. Yamaoka, Y. Mori, H. Hasegawa, K. Sato, K. Yamaguchi, K. Seno, and K. Suzuki, "First demonstration of subsystem-modular optical cross-connect using single-module 6 × 6 wavelength-selective switch," J. Lightwave Technol. **36**, 1435–1442 (2018).
5. R. Essiambre and R. W. Tkach, "Capacity trends and limits of optical communication networks," Proc. IEEE **100**, 1035–1055 (2012).
6. D. J. Richardson, J. M. Fini, and L. E. Nelson, "Space-division multiplexing in optical fibres," Nat. Photonics **7**, 354–362 (2013).
7. G. Li, N. Bai, N. Zhao, and C. Xia, "Space-division multiplexing: the next frontier in optical communication," Adv. Opt. Photon. **6**, 413–487 (2014).
8. G. M. Saridis, D. Alexandropoulos, G. Zervas, and D. Simeonidou, "Survey and evaluation of space division multiplexing: from technologies to optical networks," IEEE Commun. Surv. Tutorials **17**, 2136–2156 (2015).
9. P. J. Winzer, "Scaling optical fiber networks: challenges and solutions," Opt. Photon. News **26**(3), 28–35 (2015).

10. D. Soma, Y. Wakayama, S. Beppu, S. Sumita, T. Tsuritani, T. Hayashi, T. Nagashima, M. Suzuki, M. Yoshida, K. Kasai, M. Nakazawa, H. Takahashi, K. Igarashi, I. Morita, and M. Suzuki, "10.16-peta-b/s dense SDM/WDM transmission over 6-mode 19-core fiber across the C+L band," J. Lightwave Technol. **36**, 1362–1368 (2018).
11. S. L. Woodward, M. D. Feuer, and P. Palacharla, "ROADM-node architectures for reconfigurable photonic networks," in *Optical Fiber Telecommunications*, 6th ed., Vol. VIB of Systems and Networks (Academic, 2013).
12. D. M. Marom, P. D. Colborne, A. D'Errico, N. K. Fontaine, Y. Ikuma, E. Proietti, L. Zong, J. M. Rivas-Moscoso, and L. Tomkos, "Survey of photonic switching architectures and technologies in support of spatially and spectrally flexible optical networking [Invited]," J. Opt. Commun. Netw. **9**, 1–26 (2017).
13. G. Rizzelli, G. Maier, M. Quagliotti, M. Schiano, and A. Pattavina, "Assessing the scalability of next-generation wavelength switched optical networks," J. Lightwave Technol. **32**, 2263–2270 (2014).
14. M. Niwa, Y. Mori, H. Hasegawa, and K. Sato, "Tipping point for the future scalable OXC: what size $M \times M$ WSS is needed?" J. Opt. Commun. Netw. **9**, A18–A25 (2017).
15. F.-J. Moreno-Muro, R. Rumipamba-Zambrano, P. Pavon-Marino, J. Perello, J. M. Gene, and S. Spadaro, "Evaluation of core-continuity-constrained ROADMs for flex-grid/MCF optical networks," J. Opt. Commun. Netw. **9**, 1041–1050 (2017).
16. M. D. Feuer, L. E. Nelson, K. Abedin, X. Zhou, T. F. Taunay, J. F. Fini, B. Zhu, R. Isaac, R. Harel, G. Cohen, and D. M. Marom, "ROADM system for space division multiplexing with spatial superchannels," in *Optical Fiber Communication Conference and Exposition and the National Fiber Optic Engineers Conference* (2013), paper PDP5B.8.
17. N. K. Fontaine, T. Haramaty, R. Ryf, H. Chen, L. Miron, L. Pascar, M. Blau, B. Frenkel, L. Wang, Y. Messaddeq, S. LaRochelle, R. J. Essiambre, Y. Jung, Q. Kang, J. K. Sahu, S. U. Alam, D. J. Richardson, and D. M. Marom, "Heterogeneous space-division multiplexing and joint wavelength switching demonstration," in *Optical Fiber Communication Conference* (2015), paper Th5C.5.
18. L. E. Nelson, M. D. Feuer, K. Abedin, X. Chou, T. F. Taunay, J. M. Fini, R. Issac, R. Harel, G. Cohen, and D. M. Marom, "Spatial superchannel routing in a two-span ROADM system for space division multiplexing," J. Lightwave Technol. **32**, 783–789 (2013).
19. A. C. Jatoba-Neto, D. A. A. Mello, C. E. Rothenberg, S. Ö. Arik, and J. M. Kahn, "Scaling SDM optical networks using full-spectrum spatial switching," J. Opt. Commun. Netw. **10**, 991–1004 (2018).
20. M. Jinno, "Spatial channel network (SCN): opportunities and challenges of introducing spatial bypass toward the massive SDM era [Invited]," J. Opt. Commun. Netw. **11**, 1–14 (2019).
21. R. S. Luis, B. J. Puttnam, G. Rademacher, T. A. Eriksson, Y. Hirota, S. Shinada, A. Ross-Adams, S. Gross, M. Withford, R. Maruyama, K. Aikawa, Y. Awaji, H. Furukawa, and N. Wada, "Demonstration of a 1 Pb/s spatial channel network node," in *European Conference on Optical Communication* (2019), paper PD3.5-1.
22. M. Jinno, T. Kodama, and T. Ishikawa, "Principle, design, and prototyping of core selective switch using free-space optics for spatial channel network," J. Lightwave Technol. **38**, 4895–4905 (2020).
23. M. Jinno, Y. Asano, Y. Azuma, T. Kodama, and R. Nakai, "Technoeconomic analysis of spatial channel networks (SCNs): benefits from spatial bypass and spectral grooming [Invited]," J. Opt. Commun. Netw. **13**, A124–A134 (2021).
24. H. Hasegawa, S. Subramaniam, and K. Sato, "Node architecture and design of flexible waveband routing optical networks," J. Opt. Commun. Netw. **8**, 734–744 (2016).
25. T. Ishikawa, Y. Mori, H. Hasegawa, S. Subramaniam, K. Sato, and O. Moriwaki, "Compact OXC architecture, design and prototype development for flexible waveband routing optical networks," Opt. Express **25**, 15838–15853 (2017).
26. T. Kuno, Y. Mori, S. Subramaniam, M. Jinno, and H. Hasegawa, "Experimental evaluation of optical cross-connects with flexible waveband routing function for SDM networks," in *Optical Fiber Communication Conference and Exhibition* (2021), paper Th4E.3.
27. T. Kuno, Y. Mori, S. Subramaniam, M. Jinno, and H. Hasegawa, "High-throughput and high-port-count optical cross-connents using flexible waveband routing," in *International Conference on Optical Network Design and Modeling* (2020), paper S6.4.
28. M. Koga, A. Watanabe, T. Kawai, K. Sato, and Y. Ohmori, "Large-capacity optical path cross-connect system for WDM photonic transport network," IEEE J. Sel. Areas Commun. **16**, 1260–1269 (1998).
29. T. Watanabe, K. Suzuki, and T. Takahashi, "Silica-based PLC transponder aggregators for colorless, directionless, and contentionless ROADM," in *Optical Fiber Communication Conference* (2012), paper OTh3D.1.
30. S. Nakamura, S. Yanagimachi, H. Takeshita, and A. Tajima, "Optical switches based on silicon photonics for ROADM application," IEEE J. Sel. Top. Quantum Electron. **22**, 185–193 (2016).
31. S.-L. Woodward, M.-D. Feuer, and P. Palacharla, "ROADM-node architectures for reconfigurable photonic networks," in *Optical Fiber Telecommunications*, I.-P. Kaminow, T. Li, and A.-E. Willner, eds., 6th ed. (Academic, 2013), Ch. 15, Sec. 2, pp. 686–696.
32. G. Welbrock, "Metro 100G applications and technology," in *Optical Fiber Communication Conference and Exposition and the National Fiber Optic Engineers Conference* (2013), Market Watch Panel IV: Metro 100G Applications.
33. N. Madamopoulos, M. D. Vaughn, L. Nederlof, and R. E. Wagner, "Metro network architecture scenarios, equipment requirements and implications for carriers," in *Optical Fiber Communication Conference* (2001), paper WL2.
34. T. Hayashi, T. Taru, O. Shimakawa, T. Sasaki, and E. Sasaoka, "Uncoupled multi-core fiber enhancing signal-to-noise ratio," Opt. Express **20**, B94–B103 (2012).
35. Y. Mori, C. Zhang, and K. Kikuchi, "Novel configuration of finite-impulse-response filters tolerant to carrier-phase fluctuations in digital coherent optical receivers for higher-order quadrature amplitude modulation signals," Opt. Express **20**, 26236–26251 (2012).
36. M. S. Faruk and S. J. Savory, "Digital signal processing for coherent transceivers employing multilevel formats," J. Lightwave Technol. **35**, 1125–1141 (2017).
37. D. Chang, F. Yu, Z. Xiao, N. Stojanovic, F. Hauske, Y. Cai, C. Xie, L. Li, X. Xu, and Q. Xiong, "LDPC convolutional codes using layered decoding algorithm for high speed coherent optical transmission," in *Optical Fiber Communication Conference* (2012), paper OW1H.4.
38. R. Shiraki, Y. Mori, H. Hasegawa, and K. Sato, "Design and evaluation of quasi-Nyquist WDM networks utilizing widely deployed wavelength-selective switches," Opt. Express **27**, 18549–18560 (2019).